Real Space Structure of Associating Polymer Melts

Kathleen A. Kolbet and Kenneth S. Schweizer*

Departments of Chemistry and Materials Science & Engineering, and Materials Research Laboratory, University of Illinois, 1304 West Green Street, Urbana, Illinois 61801

Received August 3, 1999; Revised Manuscript Received December 7, 1999

ABSTRACT: Microscopic polymer integral equation theory is employed to investigate the real space collective density fluctuations and interchain radial distribution function of melts of associating AB heteropolymers of various global architectures (telechelic, multiblock). The correlation functions are analyzed in detail to extract four characteristic collective structural length scales (local, intermediate, and global) which emerge due to aggregation of the minority sticky groups: multiplet size, diffuse cluster radius, microdomain period, and intermultiplet coherence length. The dependence of such quantities on temperature, chain architectures, sticky group concentration (f_B) and blockiness, chain stiffness, and monomer volume mismatch are systematically studied, and various apparent power law dependencies on temperature and f_B are deduced. A global real space scenario for self-assembly is constructed describing the emergence and thermal evolution of each structural feature in a cooling experiment. Length scale dependent effective compositions and densities surrounding a tagged minority or majority monomer are computed, and their possible relevance to multiple glass transition phenomenon in ionomer melts is discussed. Monomer volume mismatch is always found to inhibit the microphase separation process due to steric constraints which frustrate tight sticky group packing. Comparisons with scattering experiments suggest the theory provides a reliable qualitative and, sometimes, quantitative description of real space correlations in ionomer melts. Connections between the detailed predictions and qualitative physical picture provided by the microscopic theory with the phenomenological "modified hard sphere model" of ionomer melts are established.

I. Introduction

In this companion paper, we explore our theoretical predictions for the real space structure of the associating AB polymer melt models discussed in the preceding article (referred to as paper 1).[1] There are at least four reasons for pursuing a thorough understanding of the real space structure. First, additional physical insight concerning the self-assembly process, not obtainable from small-angle scattering functions, can be extracted by analyzing the *local and intermediate* length scale interchain and collective real space correlations. Second, small-angle X-ray scattering (SAXS) experiments using high-intensity synchrotron sources allow inversion of the scattering data to obtain the collective density fluctuation correlation function in real space.[2] Third, it has very recently become possible to directly image ionic aggregates using scanning transmission electron microscopy (STEM).[3] Fourth, the fundamental assumptions of prior phenomenological models of ionomer melt self-assembly and SAXS are formulated in real space.[4]

The real space PRISM theory results presented in this paper follow immediately by numerical inverse Fourier transform of the wave vector space structure factors obtained in paper 1. The real space PRISM equations and closures are now standard and are described in great detail elsewhere.[5] The explicit equations for the relevant *k*-space pair correlation functions studied here are given in section IIB of paper 1. For example, $g_{AA}(r)$ follows from Fourier inversion of eq 2.6 in paper 1. We again remind the reader that our work considers the standard pair correlation functions accessible to scattering experiments; connectivity properties of associating polymer fluids deducable from statistical objects such as the "pair-connectedness" correlation function are not addressed.

A. Real Space Structure. The fundamental predictions of the polymer reference interaction site model (PRISM)[5] theory are the *inter*chain pair correlation, or radial distribution, functions between sites of type M and M′, $\{g_{MM'}(r)\}$. Although difficult to directly measure experimentally, such quantities can be obtained in computer simulations[6,7] and contain the fundamental statistical information about ensemble-averaged intermolecular packing. Of prime interest is the sticky group pair correlation, $g_{BB}(r)$. When the sample is cooled, this function increases dramatically on a local scale and develops longer range oscillations, as B multiplets and microdomains form. The quantity $\rho_B g_{BB}(r)$, where $\rho_B = f_B\rho_m$ is the B group total number density, represents the density of B sites on *different* polymer chains at a distance r from a single tagged B group. The total number of *inter*molecular B neighbors surrounding a tagged B group within a distance R follows from simple integration:

$$N_{BB}(R) = \int_\sigma^R 4\pi r^2 \rho_B g_{BB}(r) \qquad (1.1)$$

where σ is the monomer hard core diameter. This is an ensemble-averaged quantity and does not correspond to looking only at B groups in dense clusters. The latter procedure involves a symmetry breaking of the statistical equivalence of all B groups in an isotropic fluids and could be extracted, for example, by examining many body configurations in a computer simulation[6,7] or ultrahigh-resolution microscopy images.[3,8,9]

Other measures of length scale dependent interchain coordination numbers or densities are easily computed from the radial distribution functions. Knowledge of the $\{g_{MM'}(r)\}$ is also essential for quantifying the local interchain collision rate and forces on a molecular level,

10.1021/ma991292v CCC: $19.00
Published on Web 01/27/2000

and serve as equilibrium input to modern microscopic statistical dynamical theories of polymer fluids and glasses. They also enter simple estimates of the gelation transition based on static percolation ideas. For example, Joanny[10] has suggested the following criterion (in our notation) for thermoreversible network formation in ionomer fluids

$$N_{BB}(R^*) \cong 1.5 \tag{1.2}$$

where R^* is a separation within which two sticky B groups are presumed to form a "cross-link".

Real space collective density fluctuations of the sticky groups consist of intrachain and intermolecular parts[5]

$$S_{BB}(|\vec{r} - \vec{r}'|) = \langle \delta\rho_B(\vec{r})\delta\rho_B(\vec{r}')\rangle = \rho_B\omega_{BB}(|\vec{r} - \vec{r}'|) + \rho_B{}^2 h_{BB}(|\vec{r} - \vec{r}'|) \tag{1.3}$$

where $\delta\rho_B = \rho_B(r) - \rho_B$, and $h(r) = g(r) - 1$. Standard expressions analogous to eq 1.3 apply for the AA and AB correlations.[5] For end-functionalized telechelics (especially $N_B = 1$), the BB collective and interchain pair correlations will be closely related, but for multiblocks the presence of B groups along the entire polymer chain results in larger differences.

The density fluctuation correlation function $S_{BB}(r)$ decays to zero over a characteristic length scale beyond which the concentration of B monomers is spatially homogeneous. For a homopolymer fluid, or associating polymer melt in the high temperature athermal limit, this characteristic length scale is short, on the order of a monomer size in a dense, nearly incompressible liquid. However, in a strongly microphase-separated ionomer melt, $S_{BB}(r)$ will decay in a slower damped oscillatory manner with a period controlled by the microdomain spacing, D, and decay envelope controlled by a "coherence length," ξ_{coh}. Two other structural length scales of *intermediate* size are expected to be present in $S_{BB}(r)$. The B group density is *enriched* relative to its bulk average value within a spherical region of radius R_C defined as

$$S_{BB}(r = R_C) = 0 \tag{1.4}$$

We refer to R_C as a "cluster radius" since it corresponds to the crossover of $\delta\rho_B = \rho_B(r) - \rho_B \to 0$ and has been emphasized in other multiphase systems such as binary polymer blends undergoing spinodal decomposition.[11] R_C does *not* correspond to the size of the small dense cluster of B groups referred to as "multiplets" in ionomer materials. Rather, we introduce another length scale r^* which, as we shall argue below, correlates well with multiplet size. It is defined as the *local* maximum ($r^* < R_C$) of BB density fluctuations weighted by the surface area geometric factor:

$$r^2 S_{BB}(r) = \text{maximum at } r = r^* < R_C \tag{1.5}$$

Emergence of the structural features in $S_{BB}(r)$ which define the length scales, r^*, R_C, D, and ξ_{coh} requires some threshold degree of physical clustering and reduced inverse temperature T_s/T to be exceeded, which is expected to depend on both the specific system and length scale of interest. A schematic drawing of a self-assembling telechelic melt and the structural length scales discussed above is given in Figure 1.

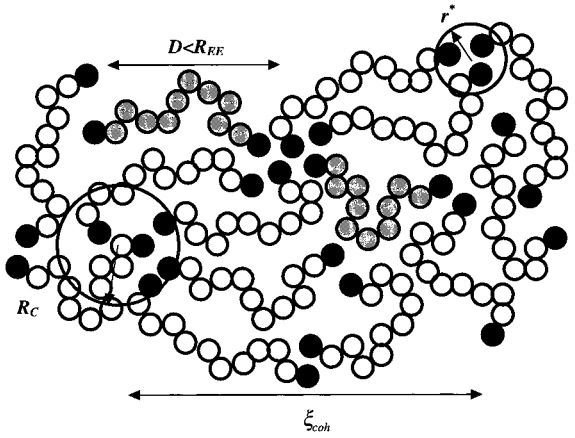

Figure 1. Schematic illustration of the various characteristic length scales and cluster formation of short telechelic ionomer melts.

Collective analogues of the length scale dependent effective coordination numbers and related quantities discussed above based on the *inter*molecular pair correlation functions can also be defined. In this paper, we focus primarily on an "effective composition" function, $\Phi_{BB}(R)$, previously introduced for diblock copolymers,[12] defined as

$$\Phi_{BB}(R) = G_{BB}(R)/[G_{BB}(R) + G_{BA}(R)]$$

$$G_{BM}(R) \equiv \int_0^R \mathrm{d}r\, 4\pi r^2[\omega_{BM}(r) + \rho_M g_{BM}(r)] \tag{1.6}$$

Physically, $\Phi_{BB}(R)$ represents the *statistically averaged fraction of monomers that are of B type inside a sphere of radius R which surrounds a given tagged B group located at the origin*. In the macroscopic $R \to \infty$ limit, this function reduces to its trivial value of the B group fraction, f_B. If the A and B monomers are randomly mixed (e.g., athermal limit), the latter limit is again achieved for that part of the effective composition which counts only *inter*chain neighbors.[12] As the fluid is cooled and B clusters form, $\Phi_{BB}(R)$ provides a spatially resolved measure of microphase separation on the length scale R. Note that for an associating polymer composed of single sticky groups ($N_B = 1$), even if all the B groups have aggregated into small spherical multiplets consisting of 10 or fewer monomers, on the most local scale one expects $\Phi_{BB}(R \cong \sigma) < 0.4-0.5$ and not unity as might be anticipated intuitively based on the mental picture of a "pure" B microcluster with a single central B monomer. This follows since even if nonpolar A groups are entirely excluded from the multiplet, most of the B groups must lie on the "surface" of a small droplet, and by definition of Φ_{BB} an *isotropic* ensemble average over all B groups is performed.

A closely related measure of clustering is the temperature and length scale dependent function

$$X_B(R;T) = G_{BB}(R;T)/G_{B,tot}(R;T \to \infty) = \Phi_{BB}(R)\{G_{B,tot}(R;T)/G_{B,tot}(R;T \to \infty)\} \tag{1.7}$$

where $G_{B,tot}$ includes *all* sites within a sphere of radius R surrounding a tagged B monomer ($G_{B,tot} = G_{BB} + G_{BA}$ from eq 1.6). $X_B(R;T)$ measures the number of B groups in a sphere of radius R centered on a tagged B site for the fluid at a temperature T relative to the *total* number of polymer sites surrounding a B group in the athermal limit. The latter is a coordination number

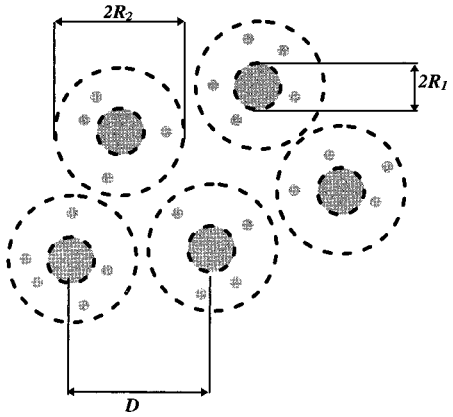

Figure 2. Schematic illustration of the liquidlike hard sphere model[4] of ionomer melts and length scales involved. The shaded regions refer to ionic-rich domains.

representative of a homopolymer melt. Hence, X_B can be interpreted as the degree to which (in a fractional sense) the environment surrounding a B group is like a dense homopolymer melt. At fixed overall density or packing fraction, the quantity in braces in eq 1.7 is expected to be nearly unity, so there will be a close relationship between $X_B(R)$ and $\Phi_{BB}(R)$.

B. Modified Hard Sphere Model. A successful, and now rather widely accepted, empirical description of the structure of ionomer melts and small-angle X-ray scattering profiles is the "modified hard sphere" model of Cooper and co-workers.[4] The underlying physical picture and fundamental structural length scales are shown schematically in Figure 2. The melt is envisioned to consist of small, dense spherical aggregates or "multiplets" of radius R_1 of essentially pure ionic material (B groups). However, these aggregates are coated with a sheath of nonpolar polymer and a distance of closest approach of the aggregates is introduced as $R_2 > R_1$. The "shell" region between R_1 and R_2 is imagined to be primarily composed of nonionic A groups, but some (small) amount of mixing with B groups must be present. The SAXS ionomer peak arises from liquidlike local order between the ionic aggregates which are modeled as a hard sphere of radius R_2 and overall volume fraction η.

In our notation, the scattering function of the modified hard sphere model is given by a product of a single aggregate contributions and an interference part due to interaggregate correlations:[4]

$$\hat{S}_{BB}(k) = (1/\nu_P)(4\pi {R_1}^3/3)^2(\Delta\rho)^2F^2(kR_1)\hat{S}_{PY}(kR_2;\eta) \quad (1.8)$$

Here, ν_P = inverse of the ionic aggregate density, $\Delta\rho$ is the electron density difference between the ionic aggregate and the sheath plus polymer matrix material, $F(kR_1)$ is the form factor for a homogeneous sphere of radius R_1, and $\hat{S}_{PY}$ is the Percus−Yevick theory static structure factor for hard spheres at a packing fraction $\eta = 4\pi R_2^3/3\nu_P$. Such a scattering function has been employed in other systems such as colloidal suspensions[13] (where the hard sphere is really a composite object) and $R_1 \cong R_2$, or diblock copolymer micelles[14] where R_1 represents the radius of the spherical minority species "droplet" and R_2 controls the degree of interpenetration of two micelles. In real space, $r^2S_{BB}(r)$ of eq 1.8 is a damped oscillatory function exhibiting a first maximum at $r \cong R_1$ associated with the "form factor" of a multiplet, a second maximum at $r \cong R_2$ correlated closely with the microdomain period, and possible higher order maxima and minima depending on the effective packing fraction η.[2,3] As we shall see, PRISM theory predicts qualitatively similar features. In practical applications to SAXS ionomer scattering data, there are many adjustable fit parameters; the most physically relevant for describing structure are[4] R_1, R_2, and η.

It is important to appreciate that the modified hard sphere model is not a microscopic description at the level of individual monomers, polymer chains, and intermolecular forces. Its purpose is to encode in a model function the presumed important morphological features of associating polymer melts and to determine (not predict) the characteristic parameters by data fitting. This contrasts strongly with our goal which is a first principles monomer-level description of the self-assembly process and pair correlation functions. However, we do believe the ideas underlying eq 1.8 are physically sensible, and connections of the model parameters with the structural length scales provided by PRISM theory (e.g., r^*, R_C, and D) are worth pursuing.

In section II, we report numerical PRISM results for telechelic melts. All our wave vector and real space information is combined in an attempt to construct a unified picture of structure on all length scales and to contrast this picture with the modified hard sphere model. Regular multiblock architectures are the subject of section III, along with a comparison with recent X-ray scattering experiments. Possible relevance of our structural results to multiple glass transitions in ionomer melts is briefly considered in section IV. Section V addresses the influence on interchain packing and microdomain formation of variable polymer stiffness and distinct A and B monomer volumes. Concluding remarks are collected in section VI.

II. Telechelics

We consider first the $N_B = 1$, $f_B = 1,2,3,5,8\%$ ($N = 200-25$) telechelic melts studied in section III of paper 1. We generally present only results for the extreme B group compositions since telechelics with intermediate values of f_B show intermediate behavior.

A. Interchain Packing. In the athermal limit, one recovers a homopolymer melt. As seen in the inset of Figure 3, a small amount of local structure is present for standard entropic packing reasons which depends very weakly on f_B or, equivalently, chain length N. Tighter contacts are formed between the chain ends on different polymers, $g_{BB}(r)$, than for AA or AB contacts. Upon cooling, B groups cluster and *three* types of strong changes in $g_{BB}(r)$ emerge; representative examples are given in Figure 3.[15]

First, on very local length scales near contact (e.g., the spatial range of the attractive Lennard−Jones-like BB potential of $\cong 1.5\sigma$), massive growth of the correlation function is found which continues to the lowest temperatures achievable with our numerical algorithm. The large BB contact values seen in Figure 3 are not unreasonable since the physically relevant quantity with regards to real space packing is the effective density, $\rho_B g_{BB}(r)$. For either the 1% or 8% telechelic at their respective values of T_{ODT}, this quantity at contact is the sensible value of $\cong 0.36\ \rho_m$ (where ρ_m is the *total* site fluid density), consistent with the formation of a small dense multiplet. The "contact value" $g_{BB}(r = \sigma)$ grows nearly linearly (see below) with the attractive

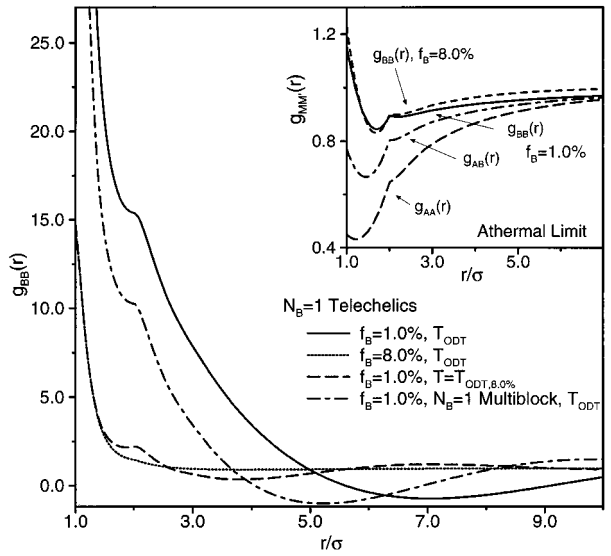

Figure 3. Interchain BB site−site pair correlation functions for $N_B = 1$ telechelics ($f_B = 1$, 8%) and a multiblock ($f_B = 1\%$) at T_{ODT}. Values of $g_{BB}(r = \sigma)$ are 60.2 and 73.0 for the $f_B = 1\%$ multiblock and telechelic, respectively. Inset: Athermal limit pair correlations for the telechelics.

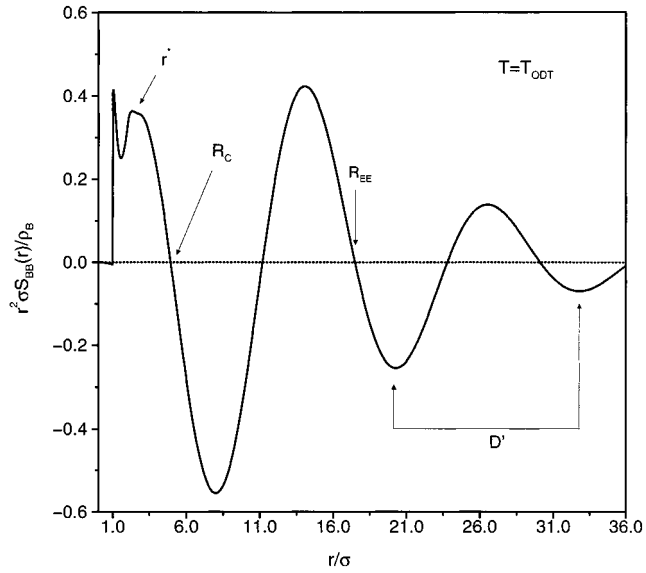

Figure 4. Dimensionless *r*-space BB structure factor multiplied by r^2 at T_{ODT} for the $f_B = 1\%$, $N_B = 1$ telechelic. r^* indicates the "multiplet" size, R_C the "cluster radius", R_{EE} the end-to-end distance of the polymer, and the microdomain period is $D' \neq 2\pi/k^*$.

strength parameter $\beta\epsilon_{BB}$ in a manner *almost identical for all values* of telechelic sticky group concentrations f_B. Thus, for the very local correlations, the reduced temperature variable, T/T_s, is *not* relevant, but instead, the absolute temperature in units of ϵ_{BB} is the controlling dimensionless energy. This finding is clearly seen in Figure 3 where $g_{BB}(r)$ for the 1% and 8% telechelics at *constant absolute* temperature are indistinguishable for $r < 1.5\sigma$. We believe this behavior makes physical sense for concentrated solutions or melts where the ability of a strong BB attraction to massively change the radial distribution function should be limited to a small region near contact on the order of the total density−density screening length or the spatial range of the Lennard−Jones attraction.[5] This feature is also relevant for crude estimates of the gelation transition based on number of local contacts. For example, at fixed ρ_m, eq 1.2 predicts that the gelation temperature is roughly proportional to the fraction of sticky groups f_B.

As also shown in Figure 3, when local clustering is compared at a fixed reduced temperature of $T = T_{ODT}(f_B)$, the more dilute sticky group telechelic displays a much stronger local enhancement of $g_{BB}(r)$ since it is at a much lower absolute temperature.

The additional two features in $g_{BB}(r)$ which emerge upon cooling are a cusplike peak or shoulder near $r \cong 2\sigma$ and long-range oscillations on the microdomain period scale. In contrast with the very local correlations, the intensity of these *inter*chain structural features correlate directly with the *reduced* temperature, T/T_s, and thus can be viewed as signatures of multiplet formation and microdomain scale order, respectively.

The potential-of-mean force between two B groups on different chains in the fluid is given by $W_{BB}(r) = -k_BT \ln g_{BB}(r)$. At low temperatures, this medium-induced potential near contact corresponds to a strong attraction of $\cong 3-4k_BT$. At very low temperatures, $g_{BB}(r)$ goes through a deep minimum[15] on a length scale of roughly half the microdomain period. Here $g_{BB}(r) \ll 1$, corresponding to an effective *repulsion* between B monomers on different coils and a potentially large repulsive barrier to separating strongly adhesive BB contacts.

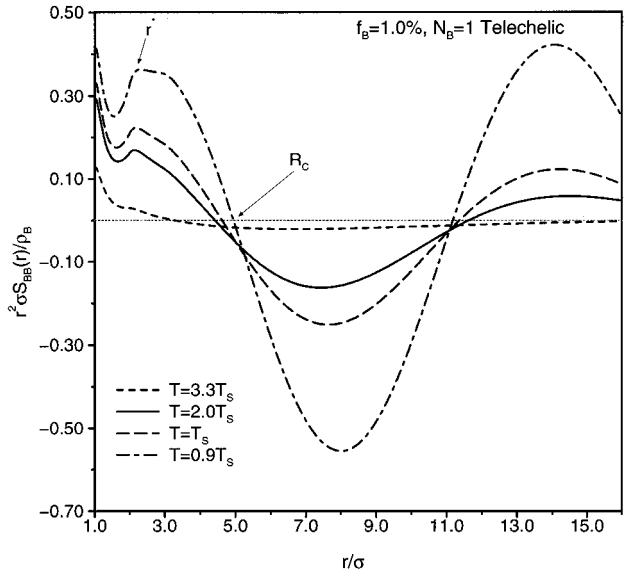

Figure 5. Temperature dependence of the dimensionless *r*-space BB structure factor (multiplied by r^2) for the $f_B = 1\%$, $N_B = 1$ telechelic.

We refrain from plotting more results for the other two radial distribution functions, $g_{AA}(r)$ and $g_{AB}(r)$. As expected, they display very little temperature dependence and no striking new features. The AA majority component correlations are almost completely *T*-independent, with slight changes increasingly detectable as f_B increases. The AB cross correlation function shows a weak increase near contact upon cooling. These changes are consistent with the *k*-space results for $\hat{S}_{AB}(k)$ in paper 1 and are a consequence of a small tendency of A monomers to be drawn into, or near the boundary of, B aggregates due to chain connectivity.

B. Collective Density Fluctuations. Examples of the dependence of the nondimensionalized version of $r^2S_{BB}(r)$ on sticky group concentration and temperature for $N_B = 1$ telechelics are shown in Figures 4−6. On length scales less than roughly half of the microdomain period, there is very little difference between $S_{BB}(r)$ and

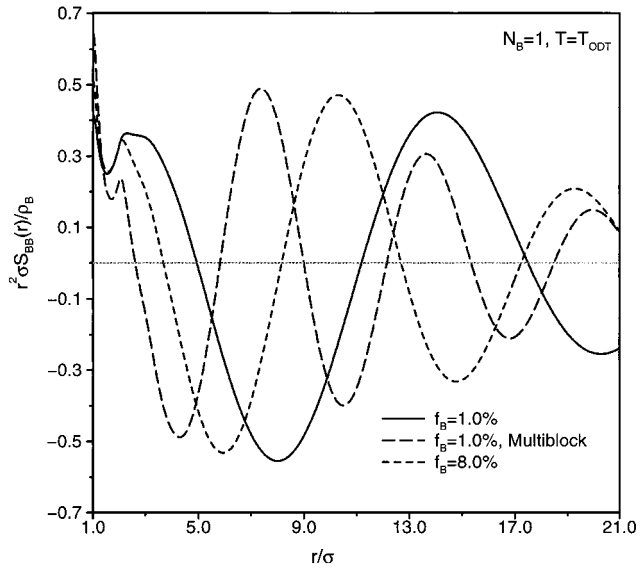

Figure 6. Dimensionless *r*-space BB structure factor multiplied by r^2 for the $N_B = 1$ telechelics ($f_B = 1,8\%$) and multiblock ($f_B = 1\%$) at T_{ODT}. Note that R_C is very dependent upon the chain architecture.

$g_{BB}(r)$ for the $N_B = 1$ end-functionalized telechelics since the intrachain contribution, $\omega_{BB}(r)$, is nearly zero on such distance scales. The characteristic length scales discussed in the Introduction: r^*, R_C, D, and the mean single chain end-to-end distance, R_{EE}, are indicated in Figure 4 for a 1% telechelic at low temperature. We find that threshold reduced inverse temperatures of $T_s/T \cong 0.4$, 0.1, and 0.1 must be exceeded before the feature that defines r^*, R_C, and D, respectively, can be detected. Thus, upon cooling, the physical picture emerges that first low amplitude, long wavelength microdomains form (as detectable via a weak peak in the small-angle scattering function $\hat{S}_{BB}(k)$) and a (diffuse) clustering length scale emerges corresponding in real space to the beginning of oscillatory behavior of $S_{BB}(r)$; at lower temperatures clear evidence of a local multiplet or aggregate size r^* appears. As f_B *increases*, lower *reduced* temperatures are required before this sequence of events commences.

Several more detailed trends for $N_B = 1$ telechelics can be identified from Figures 4−6 and the many other calculations we have performed but will not explicitly present. (1) $r^* \cong 2\sigma$ for all temperatures and all values of f_B. However, as the melt is cooled, the first maximum in $r^2 S_{BB}(r)$ becomes increasingly broader on the higher side (see Figure 5), suggesting a modest growth of mean local aggregate size and a broadened distribution. As discussed in paper 1, for our $N_B = 1$ models $\sigma \cong 5-7$ Å for typical materials, and this implies a typical aggregate radius of $r^* \cong 10-14$ Å, in qualitative accord with experimental attempts to extract this number based on Porod analysis of the SAXS profiles of telechelic melts, and also very recent STEM imaging studies.[3] (2) With cooling, the real space intensity on all length scales, the inter-multiplet coherence length (roughly identifiable with the decay envelope of the oscillatory BB density−density correlation functions), and R_C all increase, trends which make physical sense. Typically, R_C falls in the range of $R_C/D \cong 0.3-0.45$, where $D = 2\pi/k^*$ is the microdomain period. At lower temperatures, detailed analysis reveals a roughly power law growth, $R_C \propto T^{-1/3}$, and at *fixed* (but lower) values of reduced temperature T/T_s the law $R_C \propto f_B^{-0.3}$ is found. The latter scaling suggests two interesting things: (a) R_C is strongly correlated with the microdomain period which scales as $D \propto f_B^{-0.31}$ (see paper 1), and (b) at fixed absolute temperature, R_C displays a complicated nonmonotonic, but rather weak, f_B dependence due to competing effects. For example, at T/T_{ODT} of the 8% telechelic, R_C/σ varies from 2.6 ($f_B = 8\%$) to 3.0 (3%) to 2.8 (1%). (3) We also clearly find that the ratio $D/2R_C$ is a monotonically *decreasing* function of cooling, and is $\cong 1.18-1.20$ at T_{ODT} for the entire range of $f_B = 1-8\%$ telechelics. This suggests that although the average microdomain period settles down to a constant value around T_s, the spatial regions enriched in B groups, or "clusters" defined by R_C, continue to grow in size. However, they remain "nonoverlapping" in the sense that their diameter, $2R_C$, is always smaller than the mean microdomain repeat distance. (4) At low temperatures, the ratio R_C/r^* varies from $\cong 1.3-2.5$ as sticky group concentration decreases from 8% to 1%. Moreover, as seen from Figure 6, the length scale r^* is more sharply defined as sticky group composition increases, although the intensity of this feature is smaller.

The real space *majority* species density correlation function, $S_{AA}(r)$, is very weakly dependent on temperature, showing primarily features characteristic of homopolymer melts. Microdomain scale features in real space either are nonexistent or are of very low amplitude. This rather uninteresting result does have important experimental implications since SAXS experiments probe an average over all partial structure factors weighted by the appropriate scattering intensity amplitudes. In both real and wave vector space, we find that our theoretical predictions for $S_{BB}(r)$ or $\hat{S}_{BB}(k)$ are nearly indistinguishable from alternative quantities such as the total scattering with athermal homopolymer background subtracted, $S_{TOT}(r;T) - S_{TOT}(r;T \rightarrow \infty)$, where $S_{TOT} = \sum_{M,M'} S_{MM'}(r)$, or the "athermal background corrected" version of BB scattering, $S_{BB}(r;T) - S_{BB}(r;T \rightarrow \infty)$.

C. Effective Composition. Calculation of the length scale dependent effective composition $\Phi_{BB}(R)$, and the related meltlike B-fraction $X_B(R)$, follows directly from knowledge of the real space density fluctuation correlations functions and eqs 1.6−1.7. Examples are shown in Figure 7. Recall that in the $R \rightarrow \infty$ macroscopic limit, the random behavior applies, $\Phi_{BB} \rightarrow f_B$.

The main part of Figure 7a shows $\Phi_{BB}(R)$ at several values of fixed *reduced* temperature and two cases of sticky group concentration, as a function of observation length scale R. The major conclusions from these, and many other, calculations can be summarized as follows. (i) On "sufficiently small" length scales, defined as $R < D/2$, the effective compositions increase strongly with cooling, are remarkably *insensitive* to sticky group concentration at fixed *reduced* temperature, and attain a maximum value of $\cong 0.4$ for $R = \sigma$ at the lowest temperature studied. The latter value is in agreement with the geometric packing argument for a small spherical droplet presented in the Introduction. (ii) On the B multiplet r^* length scale, $\Phi_{BB} \cong 0.3$ and $X_B(r^*) \cong 0.3-0.4$ at T_{ODT}, and both are *nearly independent* of sticky group concentration. In a dense homopolymer melt, the total number of neighbors surrounding a tagged site within a distance $r^* \cong 2\sigma$ is roughly 20−25. Thus, we can estimate a "multiplet aggregation number" using eq 1.7 of $N_{BB}(r^*) = G_{BB}(R = r^*) = X_B(r^*)^*(20-25) \cong 7-10$, qualitatively consistent with arguments of Eisen-

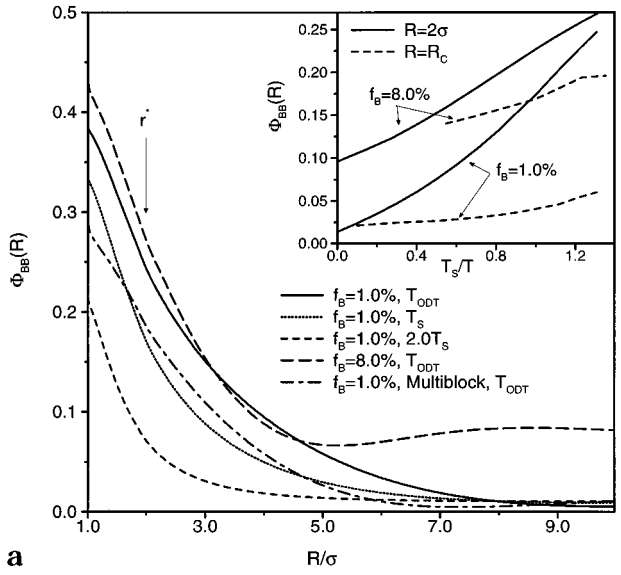

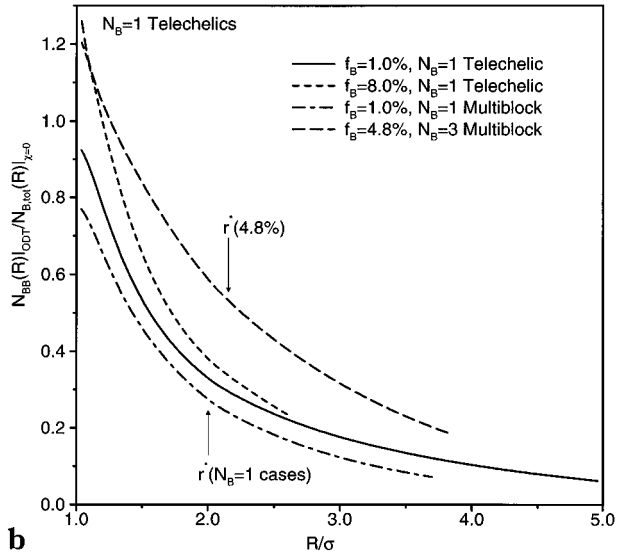

Figure 7. (a) Effective composition of the sticky groups (BB) as a function of observation length scale for the $N_B = 1$ telechelics (f_B = 1,8%) and multiblock (f_B = 1%) at several temperatures. For all these cases, $r^* \approx 2\sigma$. Inset: The temperature dependence of the effective BB composition at $R \simeq r^*$ and $r = R_c$ for the telechelics. While not shown here, for $R = R_{EE}$, the result is very nearly the athermal value ($\cong f_B$) at all temperatures. (b) Ratio of the total number of B groups surrounding a tagged B site in a spherical volume of radius R at T_{ODT} relative to the total number of all sites surrounding a B group in the athermal homopolymer limit. The end points of the curves are the R_C values for each case.

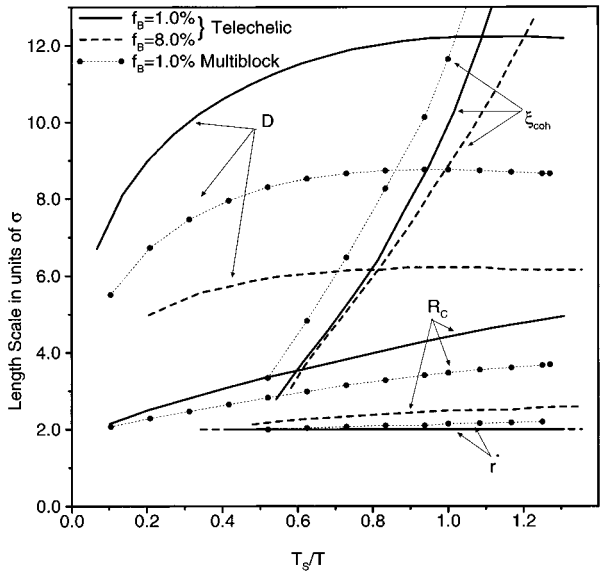

Figure 8. Characteristic length scales (in units of monomer diameter σ) vs reduced inverse temperature for several $N_B = 1$ cases. Note that the microdomain periodicity (D) saturates as $T_s/T \rightarrow 1$, r^* is nearly independent of temperature, R_C increases upon cooling, and the various structural features first become defined at different temperatures. At T_{ODT}, the coherence length ξ_{coh} = 19.8, 12.8, and 19.0 for the telechelic (f_B = 1,8%) and multiblock (f_B = 1%), respectively.

berg,[16] Cooper,[4,9] and others.[17,18] (iii) On the R_C "cluster" length scale, the effective composition falls in the window of $\cong$0.08−0.2 and is a monotonically decreasing function of f_B even at fixed reduced temperature. The B-group number density on this cluster length scale can be computed as $G_{BB}(R_c)/(4\pi R_c^3/3)$ and varies as a power law $f_B^{1/2} \propto N^{-1/2}$. (iv) On "large" length scales, $R > D/2$, oscillatory behavior is found associated with the microdomain periodicity, and Φ_{BB} is close to its bulk random value of f_B.

The inset of Figure 7a shows examples of the dependence of the effective B group composition on inverse reduced temperature evaluated on intermediate distances. The results serve mainly to reinforce the conclusions stated above and show how the temperature dependence of the local compositions weakens monotonically with increasing radius of the spatial averaging sphere R and/or sticky group fraction.

The degree to which the local environment of B groups surrounding a tagged B monomer is "homopolymer meltlike" at the ODT is presented in Figure 7b. On extremely local scales ($R \cong \sigma$), the environment of a B group is indeed "meltlike" in B monomers. On the "multiplet" r^* scale, the B-group density is 35−40% of a melt value, consistent with the picture of a multiplet as a dense droplet of $\cong$7−10 B monomers.

D. Global Picture and Comparison with Modified Hard Sphere Model. A summary plot of results for the four characteristic length scales as a function of inverse reduced temperature for two $N_B = 1$ telechelics and one multiblock (discussed below) are shown in Figure 8. The microdomain period was obtained from $\hat{S}_{BB}(k)$ via $D = 2\pi/k^*$; however, if we employ the alternative idea that D is located at the second maximum of the real space $r^2 S_{BB}(r)$, the extracted value of D' shows identical trends with T, f_B, etc., but is consistently larger by a factor of 15−25%, as also found in experiments.[2,3]

The trends in Figure 8 have been discussed previously in paper 1 and/or above. The "diffuse cluster" R_C length scale emerges *before* a local aggregate or multiplet length scale r^* is present. Note also that the microdomain period, D, saturates before the rapidly growing coherence length exceeds it. This indicates that well-defined microdomains are locally established well before strong interdomain correlations develop. At T_{ODT}, the telechelic coherence lengths in units of the microdomain period are $\xi_{coh}/D \cong 1.7$ and 2.1 for $f_B = 1$ and 8%, respectively. This ratio serves as a measure of the degree of short range order on the microdomain scale. On the basis of the PY theory, the analogous ratio for a hard sphere fluid is[19] $\cong$5 for a packing fraction close to crystallization of $\eta = 0.47$, and $\xi_{coh}/D \cong 2.5$ for $\eta = 0.37$. For a polyethylene melt at 430 K a ratio of $\xi_{coh}/D \cong 2$ is

theoretically found.[5] Thus, the degree of correlation of neighboring microdomains in telechelic melts is akin to a moderately dense hard sphere fluid or polyethylene melt.

Unfortunately, there do not seem to exist any measurements of the real space correlation functions of telechelic melts. Virtually all applications of the liquid-like hard sphere model to interpret SAXS data involve $N_B = 1$ random multiblock ionomer melts. Our results in Figure 8 (solid circles) for the $N_B = 1$, 1% regular multiblock case are qualitatively similar to telechelics. Thus, we summarize here prior applications of the modified hard sphere model to multiblock ionomer melt SAXS data, and compare with our theoretical results based on the correspondences $r^* \leftrightarrow R_1$, and $R_C \leftrightarrow R_2$, support for which we develop below.

Many studies, primarily by Cooper and co-workers,[4,9,20] have been published concerning the applications of the modified hard sphere model to interpret SAXS data for sulfonated polystyrene random ionomers with various metal cations. The major trends appear to be as follows. (1) The multiplet radius $R_1 \cong 7-10$ Å, nearly independent of temperature and ionic group fraction. The PRISM theory results are in agreement with these trends. (2) The length scale $R_2 \cong (1.7-2.3)R_1$ and is found to *decrease* with increasing ionic group composition. The latter trend suggests R_2 is correlated with the microdomain period, D. Both the magnitude of the R_2/R_1 ratio and its dependence on f_B are in qualitative agreement with our theoretical results. (3) Experiments by Chu et al.[2,3] suggest that the "clusters" defined by the length scale R_2 are not overlapping in the sense that $D/2R_2 \cong 1.2$, in agreement with our theoretical findings. (4) Early work by Yarusso and Cooper[4] used model fits to estimate that the "fraction of ionic groups in aggregates" was $\cong 30-50\%$ and independent of f_B. This is perhaps consistent with our finding that $X_B(R \cong r^*) \cong 0.35-0.4$ (see Figure 7b) *and* the idea that the experimental conditions correspond to our low temperature (T_{ODT}) model predictions.

Discussion of the seemingly good correspondence between our calculated microdomain period, D, and coherence length with small-angle scattering experiments was presented in paper 1.

E. Blocky Telechelics and Surfactants. As in paper 1, we have carried out numerical studies of the consequences of an increased sticky group block length $N_B = 3$ and the $N_B = 1$ monotelechelic or surfactant architecture. We again find no significant difference between $N_B = 1$ telechelics and surfactants when compared at fixed sticky group fraction. Hence, we focus on summarizing the similarities and differences of $N_B = 1$ and 3 telechelics.

Figure 9 contains a few examples of the behavior of $g_{BB}(r)$ for a sticky group fraction of 3%. Comparison with Figure 3 shows that the same gross qualitative features are present at low temperatures, but with some modest differences. The inset of Figure 9 shows the reduced thermal dependence of the most local aspect of the BB packing is qualitatively the same, but the magnitude and rate of growth of the blocky telechelic contact value is significantly smaller. At fixed *absolute* temperature, the blocky telechelic shows more clustering and microdomain order than its $N_B = 1$ analogue.

In contrast to the $N_B = 1$ cases, we find (not plotted) that $g_{BB}(r = \sigma)$ for blocky telechelics is now nonnegligibly, but weakly, dependent on sticky group concentration at fixed *absolute* temperature, increasing roughly as $f_B^{0.2}$. Moreover, in the crossover found for $N_B = 1$ telechelics from $g_{BB}(r)$, depending largely on absolute T to reduced temperature with increasing separation, r becomes shifted to smaller values of separation. For example, already by $r \cong r^* \cong 2\sigma$, we find that the blocky telechelic BB pair correlation function is being controlled by the reduced temperature T/T_s. These changes in behavior seem understandable as a consequence of the blocky B group multiplets now having a larger volume-to-surface ratio and containing "interior" groups as opposed to their $N_B = 1$ analogues.

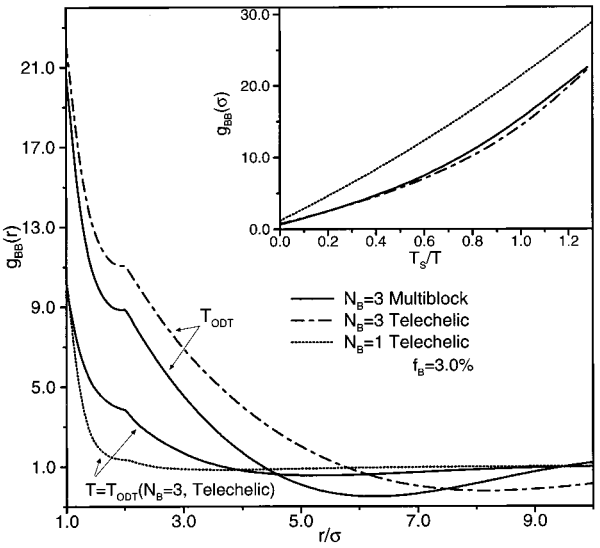

Figure 9. Interchain pair correlation functions of the sticky groups (BB) for the $f_B = 3\%$, $N_B = 3$ telechelic and multiblock at T_{ODT}, and the multiblock and $N_B = 1$ telechelic at constant $\beta\epsilon_{BB}(T = T_{ODT}(N_B = 3$ telechelic)). Inset: $g_{BB}(\sigma)$ for the same cases as a function of reduced temperature.

The AA majority component $g_{AA}(r)$ behaves the same as for the $N_B = 1$ case, although small qualitative differences appear for $g_{AB}(r)$. The contact value of this AB cross correlation decreases with cooling, in contrast to the small increase found for the $N_B = 1$ telechelics. This behavior is consistent with the significant qualitative differences between $N_B = 1$ and 3 telechelics found in low wave vector $\hat{S}_{AB}(k)$ (see Figure 12 of paper 1) and reflects the enhanced purity and reduced AB interfacial contacts when the sticky B groups can cluster as a block of three connected monomers.

Examples of the real space density fluctuation correlation functions of blocky telechelics at low temperature are shown in Figure 10. In contrast with the $N_B = 1$ analogues, the local multiplet size r^* *does* increase significantly with cooling in the low-temperature regime between T_{ODT} and T_s, in a manner which is stronger for lower sticky group concentrations (see also Figure 12). The multiplet size also decreases as a weak power law with B group fraction f_B; for example, r^*/σ varies from 2.93 (4.14) to 2.02 (2.40) as f_B increases from 1% to 8.6% at $T = T_s(T_{ODT})$. The absolute magnitude of the blocky telechelic "cluster size" R_C is, of course, larger than for its $N_B = 1$ analogue, but its dependence on f_B at fixed reduced temperature is unchanged. At fixed absolute temperature, R_C is found to increase weakly as the sticky group concentration decreases (e.g., 15% increase going from $f_B = 8.6-1.0\%$) The ratio $R_C/r^* \cong 1.8$ nearly independent of B group composition, in strong contrast to its $N_B = 1$ analogues where this ratio grows significantly from 1.3 to 2.5 as f_B increases.

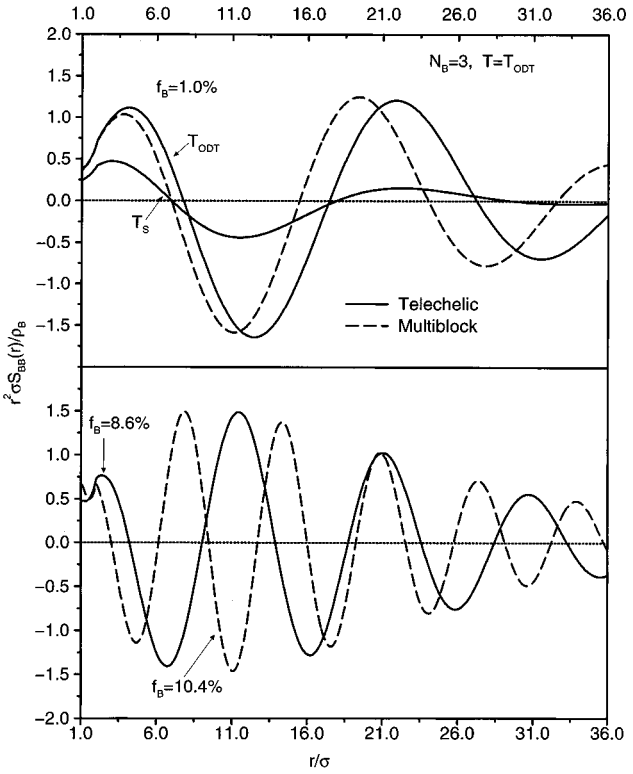

Figure 10. Dimensionless r-space BB structure factor (multiplied by r^*) for $N_B = 3$ telechelics and multiblocks at T_{ODT} and in one case at T_s.

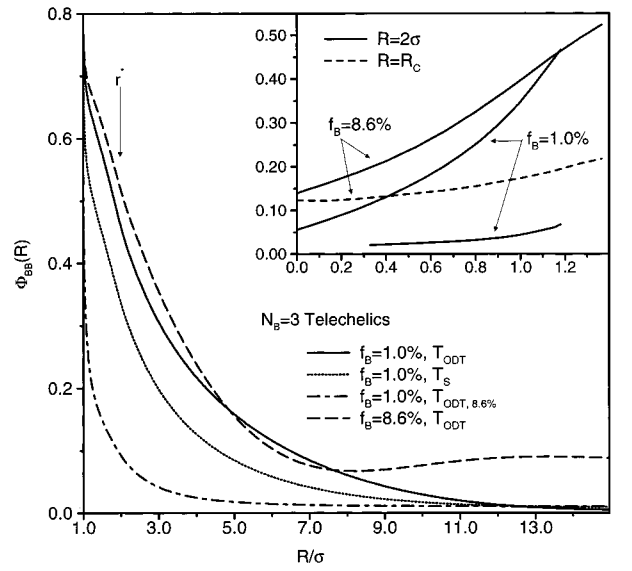

Figure 11. Effective composition of the sticky groups (BB) for the $N_B = 3$ telechelics ($f_B = 1,8.6\%$) at several temperatures vs R/σ. For all these cases, $r^* \approx 2\sigma$. Inset: Temperature dependence of the effective composition at $R \cong r^*$ and R_C for the telechelics. While not shown, for $R = R_{EE}$ the result is very nearly the athermal value at all temperatures.

Figure 11 shows examples of the effective B group composition. Comparison with Figure 7a shows that "purer" B clusters are formed, due simply due to the blockiness and enhanced ability of B groups to avoid contacts with A monomers. However, all the basic trends remain the same.

Example summaries of the all the trends discussed above are contained in the characteristic length scale plot for a 1%, $N_B = 3$ telechelic in Figure 12, which can be contrasted with its $N_B = 1$ analogue in Figure 8.

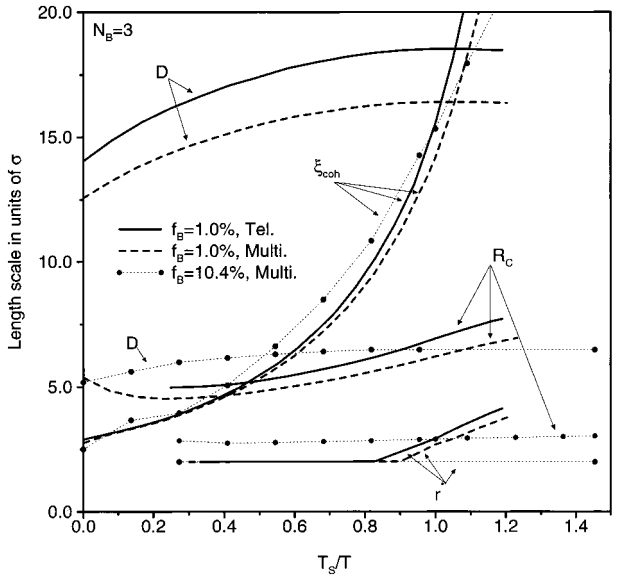

Figure 12. Characteristic length scales for several $N_B = 3$ cases vs reduced inverse temperature. Note that the microdomain periodicity (D) saturates as $T_s/T \rightarrow 1$ and r^* is *not* independent of temperature at low temperatures. The coherence length, $\xi_{coh} \rightarrow 26.1$, 25.1, and 30.0 for the telechelic and multiblocks ($f_B = 1,10.4\%$), respectively, at $T \approx T_{ODT}$.

III. Multiblocks

A. Model Calculations. As in paper 1 (section IV), a large number of model multiblock melts were studied with variable $N_B = 1,3,5$ and $f_B = 0.9-10.4$. Here, we summarize our real space findings primarily for a few selected cases. Real space results for the 1%, $N_B = 1$ (variable f_B, $N_B = 3$) multiblocks are shown for $g_{BB}(r)$ in Figure 3 (9), for $r^2S_{BB}(r)$ in Figure 6 (10), and for $\Phi_{BB}(R)$ in Figure 7, and a length scale summary is given in Figure 8 (12). There is no detectable real space microdomain structure in the athermal limit in the sense that the local multiplet feature at r^*, cluster size scale R_C, and microdomain scale oscillations are all *not* present in $r^2S_{BB}(r)$.

Relative to the analogous telechelics, the basic message is again that (even at fixed T/T_s) multiblocks consistently show reduced clustering as indicated by smaller $g_{BB}(\sigma)$, R_C, effective BB composition, et cetera, as expected due to the enhanced steric constraints to forming tight clusters. However, there are exceptions; for example, the microdomain coherence lengths of telechelics and multiblocks compared at fixed B-group composition and reduced temperature show that multiblocks exhibit a longer range correlation in their liquid like ordering (Figures 8 and 12). Other more detailed trends of the *local* interchain packing include: (i) At constant T/T_s, the multiblocks display a weaker dependence on sticky group block length than the analogous telechelics; (ii) a qualitative, but subtle, difference is that, at constant absolute temperature, as the sticky group fraction increases the contact value of $g_{BB}(r)$ *decreases* slightly, the *opposite* of the behavior found for telechelics.

Analysis of $S_{BB}(r)$ *at constant reduced temperature* reveals the following trends. (i) R_C follows the same $f_B^{-1/3}$ law as for telechelics, but the absolute magnitude of R_C is smaller (see Figures 6, 10, and 12). (ii) From Figure 12, it is evident that, at high temperatures, R_C *increases weakly upon heating*, in qualitative contrast with telechelic behavior (see Figure 8). However, this

behavior is at higher reduced temperatures than the point at which R_C is even defined for telechelics. (iii) The ratio $2R_C/D$ at the ODT is remarkably insensitive to associating group concentration and B block length. For $f_B = 0.9-10.4\%$ and $N_B = 1$, 3, and 5 models, this ratio varies only over the range of 0.85−0.94 (increases weakly with f_B). (iv) The "multiplet radius" r^* is the same or somewhat smaller than the telechelic value (see Figures 6, 10, and 12), although there are systematic differences. For example, the $N_B = 1$, 1% multiblock has $r^* \cong 2\sigma$ and $R_C \cong 4.2\sigma$ at the ODT, so $R_C/r^* \cong 2.1$. On the other hand, the $N_B = 3$ multiblocks differ from this behavior and the analogous telechelics in the sense that, at the ODT, $r^*(f_B) \cong 2\sigma$ for $f_B > 5\%$ but increases to 3.8σ for $f_B = 0.9\%$. However, R_C changes similarly so the ratio R_C/r^* is not very sensitive; at the ODT, R_C/r^* varies only over the range of $\cong 1.5-2.0$ for $f_B = 0.9-10.4\%$. (v) *At fixed absolute temperature*, the multiblocks show a *much stronger* dependence of R_C on sticky group composition than the telechelic melts; for $N_B = 3$ multiblocks, the length scale actually *increases* as f_B *decreases* despite the fact that the systems are moving away from their ODT. For example, at a fixed $T = T_{ODT}$ ($f_B = 10.4\%$), R_C/σ increases from ≅3.0 to 4.8 as f_B decreases from 10.4% to 0.9%. This trend agrees with experimental data analysis based on the liquidlike model of Cooper et al.[4] if one again identifies R_C with R_2. But this trend is *not* seen for the $N_B = 1$ telechelic where R_C is almost constant under isothermal conditions.

Analysis (see Figure 7, for example) of the multiblock $\Phi_{BB}(R)$ shows the same basic trends with changing temperature, observation size R, and sticky group concentration f_B as found for the telechelics. The notable differences are as follows: (i) At small values of $R < r^*$, and constant N_B, f_B, and T/T_s, the multiblocks show *less* pure B aggregates in the sense that $\Phi_{BB,TELECHELIC}/\Phi_{BB,MULTIBLOCK} \cong 1.34$. (ii) Of course, at constant absolute temperature a much smaller value of effective B composition is found on all length scales since the multiblocks have a higher apparent spinodal temperature than their corresponding telechelics (see Figure 9 and Figure 5 of paper 1).

Finally, the majority species density−density correlation function, $S_{AA}(r)$, is generally uninteresting in the sense that it does not exhibit the multiple features present in $S_{BB}(r)$ indicative of physical clustering and microdomain formation. The AA fluctuations (not shown) resemble homopolymers in the sense that they are short range, nearly monotonically decaying. We have also examined the dimensionless difference function, $r^2\sigma[S_{AA}(r) - S_{AA}(r)|_{\chi=0}]/\rho_A$, to extract the (weak) influence of B cluster formation on AA correlations. For example, for $N_B = 3$ multiblocks, one finds three local, highly damped oscillations at $r/\sigma \cong 1$, 2, and 3 and a long wavelength oscillation; however, the amplitudes of these features are very small, typically 1−2 orders of magnitude less than their BB analogues even at the ODT, consistent with the weak low-angle scattering peaks in $\hat{S}_{AA}(k)$ described in paper 1.

B. Comparison with Experiments. Although most experiments have been on random multiblocks, there does exist a small number of studies on a family of *regular* multiblock ionomer melts composed of sulfonated polyurethane-based polyol materials.[20] Qualitatively similar results were found: $R_1 \cong 10-15$ Å, $R_2/R_1 \cong 1.7-2.0$, and $D \cong 2R_2$, and *at fixed temperature*, both R_1 and $R_2 - R_1$ increase with decreasing ionic group concentration. All these trends seem qualitatively consistent with our periodic multiblock theoretical results described above, including the *growth* of R_2 (analogue of our cluster size R_C) with decreasing sticky group concentration at *fixed* absolute temperature and theoretical values of R_C/r^* in the range 1.5−2.0. Two temperature studies over the range of 25−225 °C have also been performed. For a Cd-neutralized material, both R_1 and R_2 decreased by roughly 15% upon heating.[20] For the analogous Zn-neutralized material, a similar change was observed up to 155 °C but then reversed upon further heating.[20] Very recent direct imaging experiments on a ≅1% Zn-neutralized E/MAA random multiblock copolymer material found spherical ionic aggregates of radius ≅13 Å.[3]

Real space correlation function analysis of SAXS data on sulfonated polystyrene random ionomer melts of $f_B \cong 4.5$ and 7.4 mol % have been carried out by Chu and co-workers.[2] The standard background homopolymer correction was applied. In addition, the contribution of the real space consequences of the excess low-angle upturn in the scattering function was subtracted from the data in order to extract the "structural" component of the collective correlations, $S_{Str}(r)$.[2a] The observations of more than two maxima and minima in the experimental correlation functions plotted as $r^2S_{Str}(r)$ argued strongly for the superiority of the modified hard sphere model[4] relative to the intraparticle interference "core−shell" model. Detailed analysis of the $r^2S_{Str}(r)$ data revealed four maxima and three minima for the 4.5% material. For the Zn-neutralized sample, from Figure 14 of ref 2a it can be seen that the maxima were located at ≅8, 42, 75, and 100 Å and minima at ≅23, 61, and 89 Å. These numbers are subject to error bars of a few angstroms, which increase at larger distance due to the reduced amplitude and increased breadth of the real space scattering features. Very similar results were found for the Na-neutralized sample.

A PRISM calculation for a 4.8%, $N_B = 3$ multiblock[2a] was carried out to make contact with this experiment. Results in the two plotting formats examined in the experiments are shown in Figure 13 at several reduced temperatures and are virtually identical to background corrected version based on $S_{BB}(r;T) - S_{BB}(r:T \to \infty)$.[21] Following the same mapping procedure employed in paper 1, we require that the space-filling volume of the small B group block equals that of a real polystyrene monomer, thereby yielding $\sigma \cong 4$ Å. Thus, at T_{ODT}, the results in Figure 13a yield maxima at ≅8, 42, 76, and 110 Å and minima at 24, 58, and 92 Å. Although perhaps fortuitous, these results are in agreement with experiment to within the uncertainties in the data.[2] In the both the data and theoretical calculation, the separation between nearest extrema fall in the rather narrow range of 14−18 Å, a number somewhat less than twice the microdomain period as defined from the wave vector space scattering function.

The second maximum in a plot such as Figure 13a is often interpreted as defining the microdomain period length scale. In the experiment, it was located at a value roughly 25% larger than the $D = 2\pi/k^*$ computed from the k-space profile,[2a] while we find a 20% enhancement from Figure 13 and the corresponding $\hat{S}_{BB}(k)$ profile (not shown). Fits of the experimental data to the modified hard sphere model found a $R_2/R_1 \cong 2$ and $D/2R_2 \cong 1.2$, in good accord with our theoretical results of $R_C/r^* \cong 2.1$ and $D/2R_C \cong 1.1$. Such agreement again suggests an intriguing correspondence between our

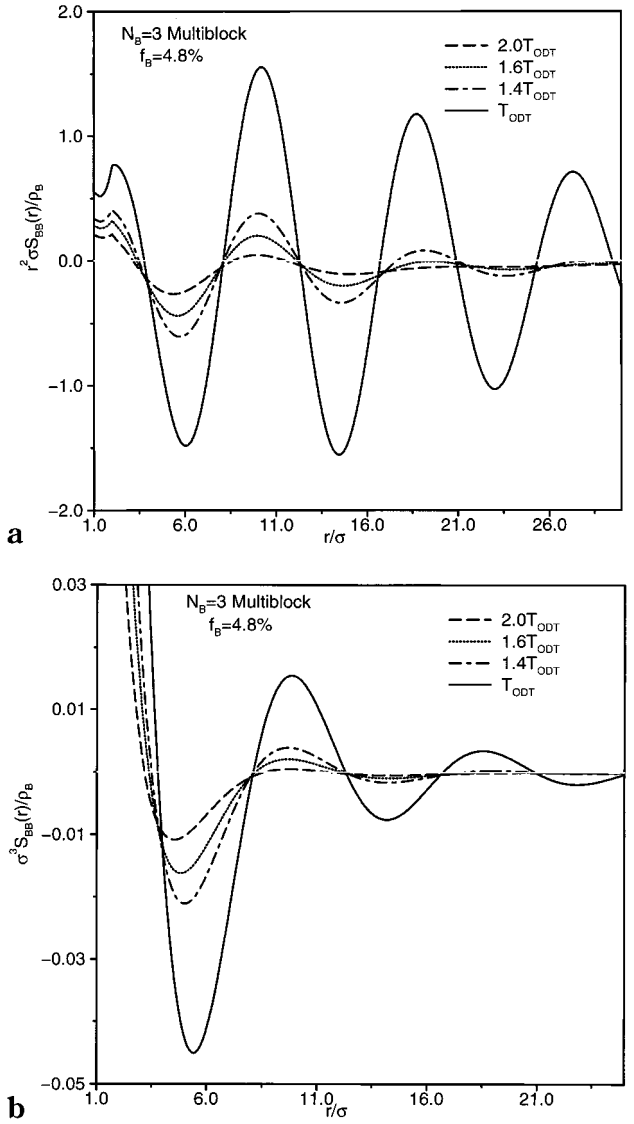

Figure 13. (b) Dimensionless r-space BB structure factor ((a) multiplied by r^2) for $N_B = 3$, $f_B = 4.8\%$ multiblock at several temperatures.

microscopically defined length scales r^* and R_C, and the fit parameters R_1 and R_2 of the modified hard sphere model.[4]

Summarizing, we appear to obtain near quantitative agreement with almost all features of these experiments,[2] with no real fitting parameters. One quantitative discrepancy is the relative amplitudes of the oscillations in the experimental and theoretical $r^2S(r)$. Normalizing to unity for the first maximum, Chu et al.[2a] found maxima intensities of 1.0, 0.34, and 0.13 with increasing r, and a first minima of relative intensity 0.68. Higher order maxima and minima were sufficiently weak that reliable estimation of their relative amplitudes from the published data was not possible. Comparing these experimental relative amplitudes to Figure 13a reveals a significant difference. There are several possible origins of this difference, including experimental resolution issues and the adequacy of our simple tangent bead semiflexible chain model.

A careful temperature study of the real and wave vector space correlation functions over the range of 25−300 °C was performed on the 7.4% Zn−SPS material.[2b] This corresponds to a change of our fundamental theoretical parameter $\beta\epsilon_{BB}$ by a factor of almost 2.

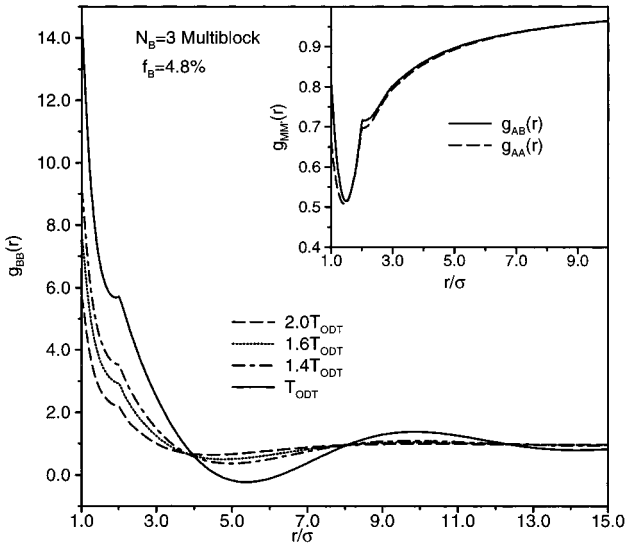

Figure 14. Interchain pair correlation functions of the sticky groups (BB) for the $N_B = 3$, $f_B = 4.8\%$ multiblock at several temperatures. Inset: The AA and AB correlation functions at T_{ODT}. While the athermal values of these functions are not shown, they would differ less than 1% from the ODT values.

Corrections for thermal expansion were applied in an attempt to extract thermally induced microstructural changes, but subtraction of the low-angle upturn scattering was not carried out. The SAXS profile in k-space dramatically decreased in intensity and broadened with increasing temperature, and the domain size became smaller by roughly 10%.[2b] At high temperatures, the real space correlation function $S(r)$ showed indications of losing its oscillatory character, perhaps indicative of strong reduction of the physical association into multiplets. The absolute magnitude of the intensity difference between the second maximum (at ≅35 Å) and the first minimum (at ≅20 Å) decreased dramatically by a factor of ≅5−8 upon heating from 25−300° C. On the basis of identifying our theoretical T_{ODT} with room temperature, all these trends seem to be in good accord with our results in Figure 13. In particular, from Figure 13b, it is evident that the absolute magnitude of the intensity difference between the second maximum and first minimum of $S_{BB}(r)$ decreases by a factor of ∼6 when the temperature is doubled, consistent with the experiment.[2b]

Figure 14 presents the corresponding predictions for the interchain radial distribution functions. Note the near identical nature of $g_{AA}(r)$ and $g_{AB}(r)$ and their near independence on temperature, consistent with the idea that the monomers of the majority phase remain in a nearly unperturbed homopolymer-like state of organization. This conclusion is reinforced by examining the real space AA density fluctuations, $S_{AA}(r)$, both in a direct manner and in a athermal background subtracted format multiplied by r^2. We find that (not shown) the local, damped AA density fluctuations which control the wide-angle scattering are almost completely insensitive to temperature, with deviations from the athermal behavior of at most of 1% at T_{ODT}. On the microdomain scale, oscillations do emerge at low temperatures, but are at least 2 orders of magnitude smaller in amplitude than those found for the analogous BB correlations.

IV. Local Densification and Glass Transitions

An intriguing feature of dense ionomer materials is the strong influence of the aggregate formation on

elevating the glass transition temperature For example, for a ≅6% sulfonated polystyrene (SPS) melt, T_g is increased by roughly 20 deg above the pure polystyrene value of 100 °C.[22] Moreover, if the ion content is "high enough" (dependent on architecture), then two distinct glass transitions are observed. For example, for ≅6% Na−SPS material a second glass transition is observed at ≅210 °C.[22] Both glass transition temperatures increase monotonically with ionic group concentration. A fundamental understanding of this phenomenon is lacking, although interesting "dynamic percolation/clustering" ideas have been suggested by Eisenberg.[16]

The glass transition temperature of homopolymers is well-known to increase strongly with applied pressure or equivalently increased density. For example, application of 1000 atm (corresponding to roughly a 1% increase in density) of pressure to polystyrene (PMMA) melts raises T_g by 31 (22) deg.[23] Moreover, one often thinks of the glass transition in terms of a length scale, or size, of "cooperatively rearranging regions". Estimates of the diameter of the latter fall in the typical range of 2−3 nm, corresponding to radii of ≅ $2-3\sigma$ in terms of our chain models.[23] Our theoretical results can be employed to estimate a length scale dependent density surrounding A or B groups, $\rho_M(R)$, which might carry useful information concerning local dynamics and thus perhaps the glass transition. The effective *total* number density in a spherical region of radius R surrounding a site of type B is

$$\tilde{\rho}_B(R) = \frac{3}{R^3}\int_\sigma^R r^2\, dr[\omega_{BB}(r) + \rho_B g_{BB}(r) + \omega_{BA}(r) + \rho_A g_{BA}(r)] \quad (4.1)$$

and the analogous expression for $\tilde{\rho}_A(R)$ follows from interchanging A and B labels in this equation. In the limit $R \to \infty$, one recovers the bulk total site number density, $\tilde{\rho}_M \to \rho$. Of primary interest is how different this quantity is compared to the corresponding unfunctionalized homopolymer melt, which has no clusters or microdomain order. The latter can be identified with the athermal limit of our model. Thus, we introduce the ratio, or density enhancement factor, $F_M(R;T)$, to quantify this local density enhancement:

$$F_M(R;T) = \tilde{\rho}_M(R;T)/\tilde{\rho}_M(R;T \to \infty) \quad (4.2)$$

In the $R \to \infty$ bulk limit ($R > D/2$ in practice), these fractions reduce to unity.

Examples of our predictions for these spatially resolved density enhancement factors are shown in Figure 15 for the low-temperature ODT situation corresponding to strong clustering and microdomain order. Even on the length scale of R≅$4-6\sigma$, there are significant enhancements of local density surrounding the sticky groups (≅2−10%). Local densifications around B group clusters of this magnitude would seem to easily translate into elevations of T_g on the order of 100 deg observed experimentally.[23] We speculate such enhancements could correlate with the higher temperature, second glass transition often described as due to mobility-restricted "clusters".[16] The dependence of this local density enhancement on chain architecture, sticky group fraction, and observation length scale is complicated.

As seen in the inset of Figure 15, the local density enhancements around the majority A groups is much smaller than its B group analogue. However, values of only ≅0.5−1% could still have a significant effect on segmental scale dynamics, and thus correlate with the modest 10−20 deg elevation of the "normal" glass transition in ionomers.[16,22]

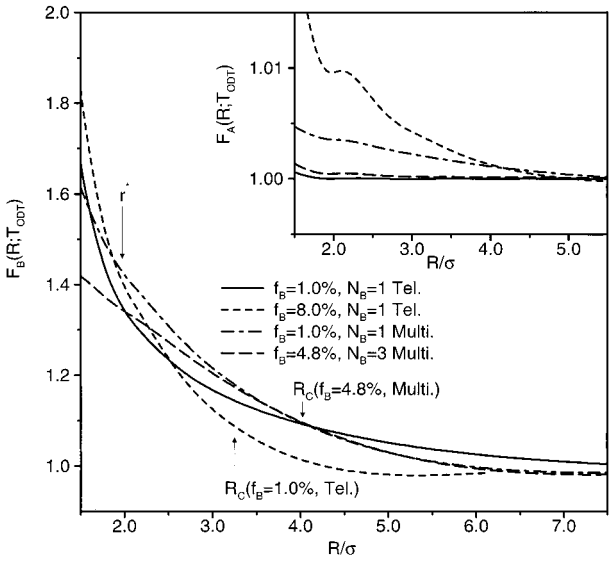

Figure 15. Density enhancement factor around a B group, $F_B(R;T)$, at $T = T_{ODT}$, for a variety of cases. The end points of each curve are at $R = D$, the microdomain periodicity. Note that $F_B(R;T) \to 1$ as $R \to D$, but that within r^* and R_C there are enhancements in the B densities. Inset: $F_A(R;T)$ for the same cases.

Definitive progress in relating local structural reorganization in ionomers to dynamical properties will require new theoretical approaches to the glass transition which connect the vitrification process with liquid structure. The modern mode-coupling theories of simple and polymeric fluids should be of use in ultimately achieving this goal.[24]

V. Effect of Chain Stiffness and Monomer Volume Mismatch

All calculations discussed so far have been performed at a fixed, "meltlike" monomer packing fraction $\eta \cong 0.3-0.4$ and for chains of a typical "flexible polymer" aspect ratio of $\Gamma = 4/3$ with A and B repeat units of identical volume ($\sigma_A = \sigma_B = \sigma$). The often dramatic consequences of changing polymer concentration by introducing neutral and selective solvent molecules has been studied and will be presented in a future publication. Here, we present a few of our numerical studies of the influence of changing backbone persistence length ($\Gamma > 4/3$) and monomer volume mismatch ($\sigma_A \neq \sigma_B$) on interchain packing and self-assembly.

A. Semiflexibility. Increasing the persistence length of the semiflexible chain model is relevant to ionomers which possess stiffer backbones for chemical structure reasons. However, such stiffening could also be "induced" by the microphase separation process. The *qualitative* consequences of a larger chain aspect ratio within PRISM theory can be largely anticipated based on elementary physical arguments. In the athermal homopolymer limit, repulsive force- driven packing effects control everything.[5] As is well-known, stiffer chains have a large R_{EE}, are more open locally, and thus form more interchain contacts ("better packing") at fixed reduced density and degree of polymerization N, thereby resulting in a larger value of $g(r)$ on very short distance scales.[5] On the basis of the RMPY−HTA closure of eq

2.18 of paper 1, this immediately implies the effective attractive cohesive interactions between B groups would be enhanced at fixed dimensionless attraction energy $\beta\epsilon_{BB}$. Thus, one expects strong physical clustering and microdomain formation to emerge at *higher* values of absolute temperature, with larger characteristic structural length scales $D = 2\pi/k^*$ and R_C. However, at constant *reduced* temperature, T/T_s, one might anticipate increased backbone stiffness will have little effect on $\hat{S}_{BB}(k)$, $g_{BB}(r)$, effective B group compositions $\Phi_{BB}(R)$, and other measures of microphase separation. The dependence on stiffness of ratios of length scales, such as D/R_{EE} and $D/2R_C$, may be both relatively weak and complicated since simultaneous changes of two properties are involved.

The scenario described above is qualitatively borne out by our numerical studies. We primarily studied $N_B = 1$ and 3 telechelics of variable sticky B group compositions ($f_B = 1-8.6\%$) and compared the results for semiflexible chains[25] of aspect ratios $\Gamma = {}^4/_3$ and 1.7 at fixed total packing fraction h. For all these model systems, the $\Gamma = 1.7$ semiflexible chain had an end-to-end distance larger by a factor of $\cong$1.2, and in the *athermal* limit the B-group contact value, $g_{BB}(\sigma)$, was $\cong$20−30% larger. These 20−30% structural differences appear to translate directly into changes of the spinodal and ODT temperatures of the stiffer chain which were all found to be enhanced by roughly 20−30%. This enhanced associating ability of the (moderately) stiffer chain predicted by PRISM should be contrasted with the simple incompressible RPA approach (see Appendix B of paper 1) which does not take into account local packing effects on interchain attractions. We find that the RPA predicts either a *much* smaller ($N_B = 3$ case) or essentially *no* increase ($N_B = 1$) of T_s of the stiffer chain melt. When compared at their respective T_s or T_{ODT}, the different stiffness chain melts displayed nearly identical values of $\hat{S}_{BB}(k^*)$ and $g_{BB}(\sigma)$. On the other hand, at T_s or T_{ODT} both the cluster size, R_C, and microdomain period, D, were larger for the stiffer chain compared to its more flexible analogue as expected, although the enhancement was significantly smaller than the R_{EE} ratio.

The ratio $D/2R_C$ at the ODT was virtually identical for the $\Gamma = {}^4/_3$ and 1.7 systems at high sticky group concentration, but was $\cong$20% larger for the stiffer chain system when the sticky groups were dilute ($f_B = 1\%$). The ratio D/R_{EE} at low temperatures for the two stiffness chains differed by a modest amount, typically 20% or less, and in a manner which depends sensitively on sticky group composition and block length. These changes of length scale ratios reflect subtle competing influences.

B. Monomer Size Asymmetry. The influence of size differences of the A and B monomers has also been studied by contrasting the behavior of $N_B = 1$ telechelic melts with $\sigma_A/\sigma_B = 0.8$, 1, and 1.25. This corresponds to cases where the A monomer volume is roughly half, equal, or twice the B monomer volume, respectively. Such models are most relevant to ionomers where two different monomers are copolymerized. However, modest monomer volume differences must exist even for functionalized homopolymers.

We employ the same semiflexible Koyama chain model[25] with a fixed total site packing fraction of 0.35 and an aspect ratio of ${}^4/_3$. Results are presented using the majority monomer diameter σ_A as the unit of length. Our primary goal is to determine the influence of monomer size mismatch on the sticky group local interchain packing and degree of microphase separation. To make a "fair comparison", we keep constant the integrated strength of the "bare" BB attractive interaction, $\int d\vec{r}\, \nu_{BB}(r) \propto \rho\sigma_B{}^3\beta\epsilon_{BB}$, by adjusting the parameter ϵ_{BB} depending on the size asymmetry ratio σ_A/σ_B. Note that this "mean-field-like" condition does *not* imply that the dimensionless temperatures for self-assembly, T_s/ϵ_{BB} and T_{ODT}/ϵ_{BB}, will be exactly the same for the different σ_A/σ_B cases (as an RPA approach would). This is because within PRISM theory the consequences of the bare attractive interactions depend in a self-consistent manner on (local) interchain packing, which will be modified for steric repulsive force reasons by the monomer volume mismatch.

Parts a and b of Figure 16 present results for $g_{BB}(r)$ and $S_{BB}(k)$ for $N_B = 1$ telechelics with $f_B = 1\%$ and 8% both in the athermal limit and at a low temperature (corresponding to the ODT of the $\sigma_A = \sigma_B$ symmetric case). Qualitatively identical trends are found for the *local* packing correlations for different B group compositions. First note that in the athermal limit, the radial distribution functions of the $\sigma_A = \sigma_B$ and $\sigma_A < \sigma_B$ (larger B end group) cases are very similar and have the "normal" shape seen for dense homopolymer melts, including a peak "at BB contact". However, when the B end groups are smaller than the majority A monomers, a dramatic change in the packing occurs. The probability of BB contacts becomes either extremely low ($f_B = 1\%$ case) or zero on the scale of our plots. The B end groups are bonded to the larger A groups, and thus sterically prevented from close contact. The largest local peak in $g_{BB}(r)$ is the AA contact distance, with a weak maximum at the arithmetic average position of $(\sigma_A + \sigma_B)/2$.

At low temperatures, all systems show significant clustering of B groups, but distinctive differences emerge. The large B group cases display $g_{BB}(r)$'s qualitatively the same as for the $\sigma_A = \sigma_B$ model, but with significantly less local degree of clustering (contact value and $r = 2\sigma$ feature) and weaker microdomain scale order as indicated by the amplitude of k^*-scale BB concentration fluctuations (see inset of Figure 16). This is understandable in terms of a packing frustration argument or interference between repulsive force packing and enthalpic cohesion considerations. The larger B groups prefer tight contacts to increase their attractive cohesive interaction, but the required characteristic packing length is 25% larger than the size of the majority A monomers. This creates an unfavorable entropic "packing problem" for the A groups, which results in the reduction of B group clustering seen in Figure 16. This phenomenon is even more dramatic for the case of smaller B end groups. Although the contact probability for B groups is enhanced relative to the athermal limit, most of the local clustering is occurring on larger length scales determined by the size of the larger A groups. Such changes in the local BB packing are expected to have important consequences for other physical properties such as multiplet cohesive energy and melt flow properties.

Summarizing, the introduction of size asymmetry frustrates the $N_B = 1$ telechelic self-assembly process on both local and microdomain length scales. Examination of the $g_{BB}(r)$'s shows that the suppression of *local* B clustering is most pronounced when the B groups are larger than the A groups for all cases of f_B considered.

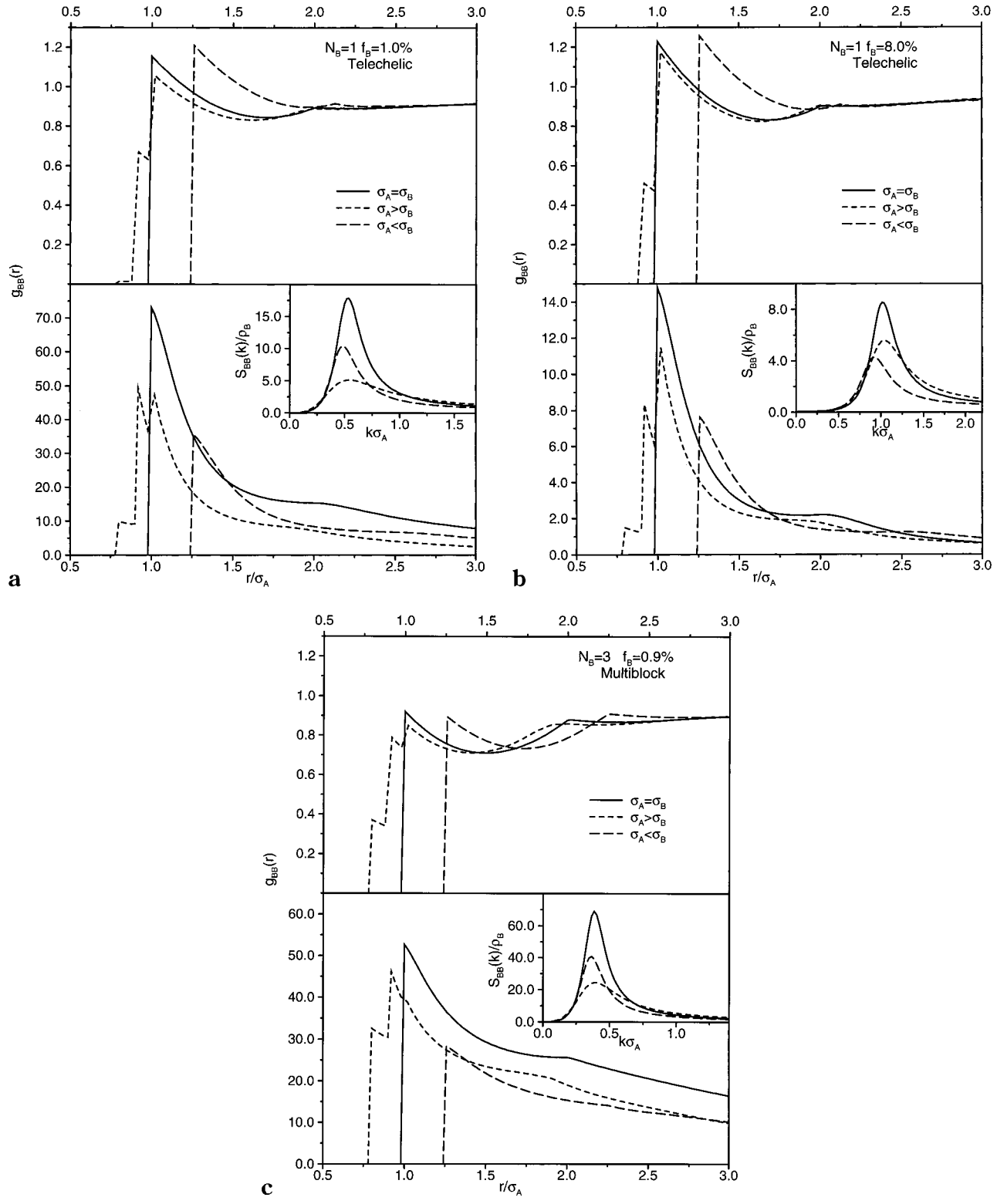

Figure 16. (a) Interchain BB site−site pair correlation functions for the $N_B = 1$, $f_B = 1\%$ telechelic with $\sigma_A = \sigma_B$, $\sigma_A > \sigma_B$, and $\sigma_A < \sigma_B$. The top figure is for the athermal temperature limit, and the lower figure is at a constant low-temperature chosen as discussed in the text: $\beta\epsilon_{BB}(\sigma_A = \sigma_B, \sigma_A > \sigma_B, \sigma_A < \sigma_B) = 45.0$, 87.8, and 23.0 Inset: The dimensionless structure factors for the three cases at low temperature. (b) Interchain site−site pair correlation functions for the $N_B = 1$, $f_B = 8\%$ telechelic with $\sigma_A = \sigma_B$, $\sigma_A > \sigma_B$, and $\sigma_A < \sigma_B$. The top figure is for the athermal temperature limit, and the lower figure is for constant low temperature of $\beta\epsilon_{BB}(\sigma_A = \sigma_B, \sigma_A > \sigma_B, \sigma_A < \sigma_B) = 9.90$, 19.31, and 5.07. Inset: The dimensionless structure factors for the three cases at low temperature. (c) Interchain site−site pair correlation functions for the $N_B = 3$, $f_B = 0.9\%$ multiblock with $\sigma_A = \sigma_B$, $\sigma_A > \sigma_B$, and $\sigma_A < \sigma_B$. The top figure is for the athermal temperature limit, and the lower figure is for constant low temperature of $\beta\epsilon_{BB}(\sigma_A = \sigma_B, \sigma_A > \sigma_B, \sigma_A < \sigma_B) = 15.3$, 29.9, and 7.85. Inset: The dimensionless structure factors for the three cases at low temperature.

However, from the $\hat{S}_{BB}(k)$ microdomain scale scattering amplitudes, ones sees that for the high sticky group fraction ($f_B = 8\%$) the larger B group system displays less microphase separation, while for the dilute $f_B = 1\%$ case the opposite trend occurs. This behavior reflects the subtle differences in the frustration of the majority species packing on the microdomain length scale due to size asymmetry depending on whether $\sigma_A > \sigma_B$ or

$\sigma_A < \sigma_B$. The BB microdomain period ($D = 2\pi/k^*$) weakly increases with the size of the B group, presumably as a direct consequence of the small increase of multiplet size and chain end-to-end distance as σ_B grows. As found for the monomer size symmetric case, changes in the telechelic $g_{AA}(r)$ and $g_{AB}(r)$ correlations (not shown) with cooling are small for the monomer size asymmetric cases considered.

We have also examined the above questions for the more blocky $N_B = 3$ telechelics, and several multiblock cases. Qualitatively similar behavior is found, although there are systematic differences. A $N_B = 3$ multiblock example ($\eta = 0.4$, $N = 1003$) for $f_B = 0.9\%$ is given in Figure 16c. For the small sticky group case, the probability of tighter contacts at $r = \sigma_B$ and $(\sigma_A + \sigma_B)/2$ is much higher in both the athermal and low-temperature regimes than for the telechelics examples. On the microdomain scale, the $\hat{S}_{BB}(k)$ profiles are ordered in the same manner as for the 1% telechelic of Figure 16a, although the reduction of microdomain scale order due to monomer size mismatch is larger for multiblocks. The latter trend would seem consistent with the physical notion that size asymmetry is more effective at disrupting B group clustering in multiblock architectures since the sticky groups are distributed all along the chain and each B group is bonded to two, not one, A groups.

VI. Discussion and Summary

The present and preceding[1] papers have constructed a microscopic theoretical description of the structure and pair correlations of dense associating polymer fluids of variable sticky group block size, concentration, and global architecture. In this final section, we attempt to summarize our findings based primarily on the real space properties. We first discuss the $N_B = 1$ telechelic systems; monotelechelic, or surfactant, architectures behave in a virtually identical manner.

In analogy with diblock copolymer melts,[26,27] from the peak small-angle BB scattering intensity, $\hat{S}_{BB}(k^*)$, we have determined two "low" temperatures which characterize self-assembly: T_s and T_{ODT}, defined in units of the system-specific sticky group attractive contact energy, ϵ_{BB}. To evaluate their physical meaning, two length scale dependent measures of local B group composition, $\Phi_{BB}(R)$ and $X_{BB}(R)$, have been analyzed. For $T \cong T_{ODT}$, we find for all $N_B = 1$ telechelics that $\Phi_{BB}(R) \cong 0.4$ at contact ($R = \sigma$), and $\cong 0.3$ on the $R = r^* \cong 2\sigma$ "multiplet" length scale. These numbers are consistent with the idea that at T_{ODT} a dense "droplet" of B groups has assembled consisting of ≈ 10 sticky monomers.[4,9,16] Further very local densification with cooling would tend to unphysically "overfill" the space, perhaps consistent in a heuristic sense with the failure of our numerical algorithm to find converged solutions to the integral equations below $T \cong T_{ODT}$. The analysis in paper 1 of the $\hat{S}_{BB}(k)$ scattering profiles at our theoretically defined "low" temperatures established consistency with many SAXS experiments.

The spatial correlations have been thoroughly analyzed in the *low*-temperature regime, and several systematic trends emerge. (i) On *most local* scales, $r < 1.4\sigma$ (the spatial range of the BB attractive interaction potential), interchain packing of sticky groups, as quantified by $g_{BB}(r)$, is controlled by the absolute magnitude of the dimensionless temperature, $\beta\epsilon_{BB}$, and *not* by a reduced temperature characteristic of microdomain scale self-assembly, T/T_s, nor by sticky group composition f_B. However, all "longer" length scale correlations are controlled by the reduced temperature with f_B-dependent *apparent* spinodal or ODT temperatures. (ii) From analysis of $r^2 S_{BB}(r)$, a characteristic local cluster of B groups, or "multiplet", emerges of nearly constant radius of $r^* \cong 2\sigma \cong 10-14$ Å. (iii) The microdomain period, D, becomes nearly constant in the low-temperature regime, well before the emergence of strong intermicrodomain correlations (characterized by the coherence length scale ξ_{coh}) in the sense that $D > \xi_{coh}$ at the temperature of onset of constant D. The "space-filling" law[18] $D \propto f_B^{-1/3} \propto N^{1/3}$ is obeyed to a very good approximation. This indicates at low temperatures that the intermicrodomain separation is smaller than the telechelic end-to-end distance $R_{EE} \propto N^{1/2}$; however, for most cases studied, these two length scales are numerically close, and a reversal of their ordering can occur at higher temperatures for short (large f_B) telechelics. (iv) In stark contrast with D, the coherence length grows strongly with cooling in the low-temperature regime, indicating increasingly long range but liquidlike ordering on the microdomain length scale. Typically, $\xi_{coh} \cong D$ at T_s, and $\cong 2-2.5$ at the ODT, corresponding to an inter-microdomain correlation length much larger than the chain end-to-end distance. The ratio ξ_{coh}/D is of a numerical size characteristic of *local* collective density fluctuations (WAXS amorphous halo) in a dense homopolymer melt.[5] (v) An intermediate "diffuse cluster radius" R_C length scale also exists at low temperatures. It precisely defines the radius surrounding a B monomer within which the concentration of sticky groups exceeds the bulk average. Upon being cooled at low temperatures, B monomers continue to weakly aggregate in the diffuse cluster sense. The ratio $2R_C/D \cong 0.6-0.9$ in the low temperature regime, corresponding to "nonoverlapping" diffuse clusters which tend to approach "close packing" at the lowest temperatures we can obtain numerical results. At low reduced temperatures, the diffuse cluster size becomes increasingly larger relative to the multiplet size as f_B increases, $R_C/r^* \cong 1.3-2.5$. (vi) The measures of length scale dependent effective B volume fractions, $\Phi_{BB}(R)$ and $X_B(R)$, increase with cooling on all length scales $R < R_C$ in a manner controlled by reduced temperature. This behavior is nearly independent of sticky group composition for small $R \cong r^*$, but on the diffuse cluster scale, it is a monotonically decreasing function of f_B at fixed reduced temperature with $\Phi_{BB}(R \cong R_C) \cong 0.08-0.2$.

Upon being heated well above the apparent spinodal temperature, the self-assembled structure breaks up "from the inside out". That is, as T increases, the local multiplet feature at r^* first disappears, and the melt consists of diffuse clusters and weak microdomains with very little intermicrodomain correlations. At these higher temperatures, the intermultiplet correlation length becomes much shorter than the microdomain period (e.g., $\xi_{coh} \cong D/5$). Eventually, the features of the collective BB concentration fluctuations which define the diffuse cluster and microdomain period vanish entirely, and a nearly homogeneous homopolymer (athermal) melt is recovered. This is in contrast with diblock copolymers which always display a weak long wavelength correlation hole scattering feature.[26,27] At all temperatures, we find little change in the AA and AB structural correlations, indicating that A monomers remain in a nearly homogeneous meltlike state.

The question of how the above scenario of $N_B = 1$ telechelic self-assembly is modified if short sticky *blocks* ($N_B = 3$) are employed has been addressed. Significant differences are found since the elementary "multiplet" unit is now larger with an enhanced volume-to-surface ratio. As expected, at fixed bare driving force, $\beta\epsilon_{BB}$, these telechelics display more clustering on all length scales than their $N_B = 1$ analogues. The multiplets are characterized by a larger value of r^*, which, in contrast with the $N_B = 1$ analogues, increases significantly with cooling in the low-temperature regime and in an increasingly dramatic manner as the sticky group composition decreases. The diffuse cluster radius R_C is larger of course, but at fixed reduced temperature displays the same f_B dependence as the $N_B = 1$ analogues. However, in contrast with the $N_B = 1$ analogues, at low temperatures the ratio R_C/r^* is nearly constant at $\cong$1.8 for all sticky group compositions. Examination of the length scale dependent effective composition function shows the B clustering is stronger than for the $N_B = 1$ case even at fixed reduced temperature, although all the basic trends for this property remain qualitatively the same.

The self-assembly behavior of multiblock architectures is less sensitive to sticky block length ($N_B = 1$, 3, 5) than their telechelic counterparts, and a bit closer to classic copolymers composed of long blocks.[26,27] For example, weak microdomain scale (correlation hole) peaks in $\hat{S}_{BB}(k)$ are found even in the athermal limit. However, thermally driven clustering is still required for the collective multiplet and diffuse cluster features to emerge; that is, nonzero threshold values of T_s/T must be exceeded. Since the sticky groups are embedded along the chain in the multiblock architecture, they experience more steric constraints for close contacts. Hence, all measures of clustering on all length scales are found to be weaker for multiblocks relative to their analogous telechelics. When compared at fixed reduced temperatures, the differences in the qualitative trends of r^*, R_C, D, etc. are small, although there are exceptions. For example, at fixed absolute temperature $\beta\epsilon_{BB}$, the multiblock diffuse cluster radius is a much stronger function of sticky group composition than found for telechelics. A dramatic consequence of this is that even at fixed temperature, R_C increases as f_B decreases, despite the fact that the latter change corresponds to moving away from the self-assembly temperature T_s or T_{ODT}. Such counterintuitive behavior seems consistent with SAXS experiments on multiblocks[9] which agree with this trend within the context of the Cooper et al. model[4] and the identification of the parameter R_2 with our R_C. The behavior of $\Phi_{BB}(R)$ for multiblocks is qualitatively the same as for telechelics although the weaker clustering of the former implies smaller enrichments of local B compositions occur.

A quantitative application of the theory for multiblocks has been performed to compare with real space data of Chu and co-workers[2] for $S_{BB}(r)$. Good agreement between theory and experiment is found for the detailed oscillatory features of the real space correlation function and its dependence on temperature over a 200 deg range.

The microscopic nature of the theory has been used to address three additional questions. The first is local densification around A and B groups driven by the self-assembly process. Large enhancements of total monomer density surrounding B groups on the 4−6σ ($\cong$20−30 Å) length scale are found at low temperatures, perhaps related to the second, much higher glass transition exhibited by many ionomer melts. Self-assembly is found to induce much weaker density enhancements surrounding the majority A monomers, but of a magnitude which is still nonnegligible regarding its possible dynamic consequences and elevation of the primary glass transition temperature. Second, a modest increase of the backbone stiffness opens up the chain to more intermolecular contacts. This results in modest enhancements of all features of the self-assembly process. Third, introducing differences in the size of A and B monomers introduces local "packing frustration", which results in a reduction of the degree of clustering and self-assembly on all length scales for telechelics and even more significantly for multiblock polymers.

Finally, further progress will require testing our theory in much more detail than presently possible. Benchmark computer simulations of dense, continuous space models of semiflexible associating polymers are required to access the accuracy of the statistical mechanical closure approximations for handling strong attractive forces and to establish the limitations of assuming unperturbed conformations under melt and concentrated solution conditions. New systematic SAXS experiments on model telechelics would be of great value to quantitatively test the microdomain scale and real space intermediate scale predictions of the theory. In particular, varying temperature, and possibly sticky group composition and block length, over a wide range could be very revealing. Neutron-scattering experiments on associating polymers where deuteration is employed to allow the majority component scattering to be measured would also be valuable since the theory makes definite predictions for such quantities which depend systematically on global architecture, temperature, and sticky group composition and block length.

Acknowledgment. This work was supported by the U.S. Department of Energy, Division of Materials Science, Grant DEFG02-96ER45439, through the University of Illinois at Urbana-Champaign, Frederick Seitz Materials Research Laboratory. Helpful discussions and/or correspondence with Professors Ben Chu, Rick Register and Robert Weiss are gratefully acknowledged.

References and Notes

(1) Kolbet, K. A.; Schweizer, K. S. *Macromolecules* 2000, 33, 1425 and references therein.
(2) (a) Chu, B.; Wu, D. Q.; Lundberg, R. D.; MacKnight, W. J. *Macromolecules* **1993**, *26*, 1000. (b) Wang, J.; Li, Y.; Peiffer, D. G.; Chu, B. *Macromolecules* **1993**, *26*, 2633.
(3) Laurer, J. H.; Winey, K. I. *Macromolecules* **1998**, *31*, 9106.
(4) Lee, D.; Register, R. A.; Yang, Z.; Cooper, S. L. *Macromolecules* **1988**, *21*, 998. Yarusso, D. J.; Cooper, S. L. *Macromolecules* **1983**, *16*, 1871.
(5) Schweizer, K. S.; Curro, J. G. *Adv. Chem. Phys.* **1997**, *98*, 1; *Adv. Polym. Sci.* **1994**, *116*, 319 and references cited therin.
(6) Khalatur, P. G.; Khoklov, A. R. *Macromol. Theory Simul.* **1996**, *5*, 877. Khalatur, P. G.; Khokhlov, A. R.; Kovalenko, J. N.; Mologin, D. A. *J. Chem. Phys.* **1999**, *110*, 6039.
(7) Khalatur, P. G.; Men'hikova, L. V.; Khoklov, A. R. *Macromol. Theory Simul.* **1997**, *6*, 317.
(8) Nguyen, D.; Zhong, X.; Williams, C. E.; Eisenberg, A. *Macromolecules* **1994**, *27*, 5173.
(9) Li, C.; Register, R. A.; Cooper, S. L. *Polymer* **1989**, *30*, 1227.
(10) Joanny, J. F. *Polymer* **1980**, *21*, 71.
(11) See for example: Hashimoto, T. In *Materials Science and Technology*; Cohn, R., Haasen, P., Kramer, E. J., Eds.; 1991; Vol. 12.
(12) David, E. F.; Schweizer, K. S. *Macromolecules* **1995**, *28*, 3980; **1997**, *30*, 5180.

(13) Russell, W. B.; Saville, D. A.; Schowalter, W. R. *Colloidal Disperions*; Cambridge University Press: Cambridge, England, 1989.
(14) See for example, Chu, B.; Wu G.; Schneider, D. K. *J. Polym. Sci., Polym. Phys.* **1994**, *32*, 2605.
(15) At very low temperatures, $T \sim T_{ODT}$, $g_{BB}(r)$ can become negative near the first deep minimum. Such unphysical behavior is well-known to occur in approximate integral equation theories. However, it is interesting to note that such behavior occurs in near coincidence with failure of the numerical iteration algorithm at low temperature and with attainment of nearly dense packing values for effective compositions and nearest neighbor BB coordination numbers. This provides some further operational support for the speculation that the temperature we define as T_{ODT} has physical significance as the point at which a "low temperature" strongly segregated structure forms.
(16) Eisenberg, A.; Hird, B.; Moore, R. B. *Macromolecules* **1990**, *23*, 4098. Eisenberg, A. *Macromolecules* **1970**, *3*, 147.
(17) Sobry, R.; Fontaine, F.; Ledent, J.; Foucart, M.; Jérôme, R. *Macromolecules* **1988**, *31*, 4240.
(18) Williams, C. E.; Russell, T. P.; Jérôme, R.; Horrion, J. *Macromolecules* **1986**, *19*, 2877.
(19) Hansen, J. P.; McDonald, I. R. *Theory of Simple Liquids*; Academic: London, 1991.
(20) Ding, Y. S.; Register, R. A.; Yang, C.; Cooper, S. L. *Polymer* **1989**, *30*, 1213.
(21) We find only very small differences on local length scales ($r < 3\sigma$) associated with density fluctuations. We have also examined the difference function based on the total scattering, $S_{TOT}(r;T) - S_{TOT}(r;T \rightarrow \infty)$, and find essentially the same behavior as presented for $S_{BB}(r)$.
(22) Weiss, R. A.; Lefalar, J. A. *Polymer* **1986**, *27*, 3. Weiss, R. A.; Fitzgerald, J. J.; Kim, D. *Macromolecules* **1991**, *24*, 1071.
(23) Sperling, L. H. *Introduction to Physical Polymer Science*, 2nd ed., J. Wiley & Sons: New York, 1992.
(24) Gotze, W.; Sjogren, L. *Rep. Prog. Phys.* **1992**, *55*, 291. Schwezier, K. S.; Fuchs, M.; Szamel, G.; Guenza, M.; Tang, H. *Macromol. Theory Simul.* **1997**, *6*, 1037.
(25) Honnell, K. G.; Curro, J. G.; Schweizer, K. S. *Macromolecules* **1990**, *23*, 3496.
(26) David, E. F.; Schweizer, K. S. *J. Chem. Phys.* **1994**, *100*, 7767 and 7784. Guenza, M.; Schweizer, K. S. *J. Chem. Phys.* **1997**, *106*, 7391. David, E. F.; Schweizer, K. S. *Macromolecules* **1997**, *30*, 5180.
(27) Bates, F. S.; Fredrickson, G. H. *Annu. Rev. Phys. Chem.* **1990**, *41*, 525.

MA991292V